Computational Materials Science 150 (2018) 353–357

Contents lists available at ScienceDirect

Computational Materials Science

journal homepage: www.elsevier.com/locate/commatsci

A self-contained algorithm for determination of solid-liquid equilibria in an alloy system

L. Yang[a,b], Y. Sun[a], Z. Ye[a], F. Zhang[a,*], M.I. Mendelev[a], C.Z. Wang[a,b], K.M. Ho[a,b,c]

[a] Ames Laboratory, US Department of Energy, Ames, IA 50011, USA
[b] Department of Physics, Iowa State University, Ames, IA 50011, USA
[c] Hefei National Laboratory for Physical Sciences at the Microscale and Department of Physics, University of Science and Technology of China, Hefei, Anhui 230026, China

ARTICLE INFO

Keywords:
Free energy calculations
Sold-liquid equilibria
Thermodynamics integration
Alchemical path

ABSTRACT

We describe a self-contained procedure to evaluate the free energy of liquid and solid phases of an alloy system. The free energy of a single-element solid phase is calculated with thermodynamic integration using the Einstein crystal as the reference system. Then, free energy difference between the solid and liquid phases is calculated by Gibbs-Duhem integration. The central part of our method is the construction of a reversible alchemical path connecting a pure liquid and a liquid alloy to calculate the mixing enthalpy and entropy. We have applied the method to calculate the free energy of solid and liquid phases in the Al-Sm system. The driving force for fcc-Al nucleation in Al-Sm liquid and the melting curve for fcc-Al and Al_3Sm are also calculated.

1. Introduction

Reliable free energy for both solid and liquid phases of an alloy is fundamental to achieving a microscopic understanding of freezing and melting phenomena, which remains a significant challenge in condensed matter physics and materials science [1]. The origin of the difficulty in free energy calculations is that free energy cannot be expressed as a simple average of a physical quantity over the phase space that can be conveniently evaluated in a single simulation with a standard sampling technique, such as Monte Carlo (MC) or Molecular Dynamics (MD) [2]. A variety of methods have been proposed for free energy calculations, emphasizing on computing the free energy *difference* between the target system and a reference system. These methods include multistage free energy perturbation [3], particle insertion/deletion [4–6], thermodynamic integration (TI) [7], Bennett analysis [8,9], weighted histogram [10], umbrella sampling [11], and adiabatic switching [12]. In addition to these equilibrium approaches, Jarzynski established a nonequilibrium equality to express the free energy difference in terms of the irreversible work along paths connecting the two systems. A path-sampling technique with the application of umbrella sampling has been formulated to improve the convergence of the original Jarzynski method [13], and has been applied on clusters [14], glasses [15] and crystalline alloys [16]. For binary fluids, alternatively, people have used relatively efficient methods such as energy partitioning method [17] and classical density-functional approach [18] to estimate the free energy.

When selecting a specific method, one strikes a balance between efficiency and accuracy according to the problem at hand. The main objective of the current paper is to develop a self-contained algorithm to *accurately* determine the free energy of both liquid and solid phases, in order to establish phase equilibria. The algorithm will be developed within the framework of TI, coupled with extensive GPU-accelerated MD simulations [19,20]. TI is based on the idea that derivatives of free energy are often well-defined ensemble averages that are measurable in a single MC or MD simulation. In this method, one evaluates the derivative of free energy along a reversible path connecting the reference system and a target realistic system. The integration of the derivative along this path gives the free energy difference between the two systems [2,7].

In principle, one can obtain the absolute free energy of solid and liquid phases by referencing to a harmonic crystal and the ideal gas, respectively, whose free energy can be analytically derived. However, it is generally not a good idea to treat the liquid and solid phases in separate frameworks when it is the free energy *difference* that controls phase stability [18]. Furthermore, many phenomena of interest such as crystal nucleation and growth occur when the liquid becomes supercooled, when it behaves so differently from the ideal gas that one needs to be very careful to obtain the required accuracy by using the ideal gas as the starting point. Here, we choose the harmonic crystal, such as the Einstein crystal [21,22] as a global initial reference system, since it can provide a reliable reference for pure solid phases in most cases. The general strategy is as follows: first, we calculate the absolute free energy

* Corresponding author.
E-mail address: fzhang@ameslab.gov (F. Zhang).

https://doi.org/10.1016/j.commatsci.2018.04.028
Received 28 November 2017; Received in revised form 12 April 2018; Accepted 13 April 2018

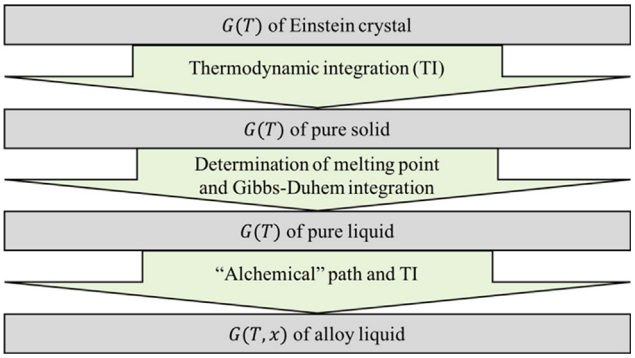

Fig. 1. Flowchart summarizing the algorithm for our free energy calculation.

of the solid phase directly using an Einstein-crystal reference; next, we determine the free energy difference between the solid and liquid phases at a specific state point; and finally, we use Gibbs-Duhem integration [23] to extend to other state points, such that all the free energy calculations are based on the same initial reference system. While the free energy difference at an arbitrary state point can be calculated by methods such as pseudosupercritical path integration [24,25], in this paper, we choose a special state point: the melting point, at which the free energy difference is zero. The accurate melting point is determined by monitoring the migration of a solid-liquid interface.

Next, we construct an "alchemical" path to transform a pure liquid to a liquid alloy, and apply TI to evaluate the mixing enthalpy and entropy during the process. Similar methods were frequently used previously to analyze affinity change upon substitution of certain atoms or functional groups in chemical or biochemical systems [26–28]. This strategy, together with a reliable method of determining solid/liquid free energy difference in single-element systems, forms a self-contained way of establishing phase equilibria in alloys. The algorithm is summarized in a flowchart shown in Fig. 1.

We choose the Al-Sm system for the current study, which is a typical member of Al-RE systems (RE: rare earth). At ~10 at% Sm, this system can form metallic glasses or nanocomposite materials with low-density-high-strength properties [29]. The evaluation of thermodynamic stability of relevant phases is necessary to understand the complicated phase selection of this system especially under supercooling, which is key to achieving the desired compositions and microstructures.

2. Computational details

All simulations are performed using the MD technique with a timestep of 2 fs, as implemented in LAMMPS GPU-accelerated package [19,20]. Systems are fully equilibrated in 500,000 timesteps in canonical ensemble (*NVT*) or isothermal-isobaric ensemble (*NPT*) with the Nose-Hoover thermostat [30,31]. The main purpose of performing MD simulations in this work is to calculate the ensemble average of certain quantities (details are shown below), which is equivalent to the temporal average under the ergodic hypothesis. The average is collected in another 500,000 timesteps after the equilibrium is reached. For efficient energy and force calculations, we use semi-empirical interatomic potential in the Finnis-Sinclair form [32], which was developed to reproduce pure Al properties, energetics of Al-Sm intermetallic alloys and Al-Sm liquid structures [33]. This potential was particularly designed to treat Al-rich alloys (at% Sm $<$ ~10%).

3. Pure fcc-Al and Al liquid

We start with the calculation of free energy of the fcc-Al phase with TI, using the Einstein crystal as a reference system. The Helmholtz free energy of a classical Einstein crystal can be determined analytically as $F_0 = 3Nk_BT\ln(h\nu/k_BT)$, with N the number of atoms, h the Planck constant, ν the vibrational frequency and k_B the Boltzmann constant. To implement TI, one generates intermediate systems with potentials $U(\lambda) = (1-\lambda)U_E + \lambda U_{Al}$, where U_E and U_{Al} stand for the potentials for the Einstein crystal and the real Al system, respectively. Then, the difference in Helmholtz free energy between the two systems can be expressed as

$$F_{Al,s} - F_0 = \int_0^1 \left\langle \frac{dU(\lambda)}{d\lambda} \right\rangle_{\lambda,NVT} d\lambda = \int_0^1 \langle U_{Al} - U_E \rangle_{\lambda,NVT} d\lambda. \quad (1)$$

In Eq. (1), the subscript s stands for solid, and $\langle\cdots\rangle_{\lambda,NVT}$ denotes the canonical ensemble (NVT) average of fcc-Al with respect to the intermediate potential $U(\lambda)$. The volume is fixed at the equilibrium volume at ambient pressure, which is determined separately via MD simulation with the real FS potential for Al under NPT conditions. In this way, the Helmholtz free energy is equal to the Gibbs free energy at the same temperature.

As an example, we show in Fig. 1 the integrand of Eq. (1) for the implementation of TI at 800 K. The vibrational frequency ν for the Einstein crystal is chosen to be 5 THz, which is close to the principal peak of Al phonon density of states [34]. The integration, performed based on cubic spline interpolation of discrete data points collected by separate MD runs (red open circles), gives the free energy difference between fcc-Al and Einstein crystal reference $\Delta F = -3.872$ eV/atom (see Fig. 2).

To calculate the free energy of Al liquid, we first determine the melting point (T_m) of fcc-Al under ambient pressure, at which the difference in Gibbs free energy between the solid and liquid phases $\Delta G = 0$. Following the method described in Ref. [35], we plot the solid-liquid interface (SLI) velocity, obtained from MD simulation for the [1 0 0] direction, as function of temperature (see Fig. 3). The melting temperature determined from these data is 915.7 ± 0.5 K, which is slightly lower than the experimental value (933 K). The Gibbs free energy difference at other temperatures is readily available by integrating the Gibbs-Helmholtz equation

$$\left[\frac{\partial(\Delta G/T)}{\partial T}\right]_P = -\frac{\Delta H}{T^2}, \quad (2)$$

where ΔH is the enthalpy change in the liquid and solid phases, or, the latent heat. The absolute free energy for Al liquid can be obtained by combining the information on solid-liquid free energy difference and the absolute free energy for the solid fcc-Al calculated previously. The final results are shown in Fig. 4

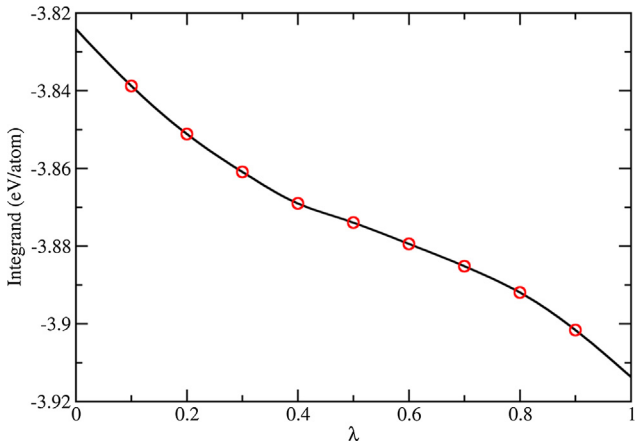

Fig. 2. The integrand of Eq. (1) for fcc Al at T = 800 K. Open circles are data points collected in separated MD runs. The solid line is a cubic spline interpolation.

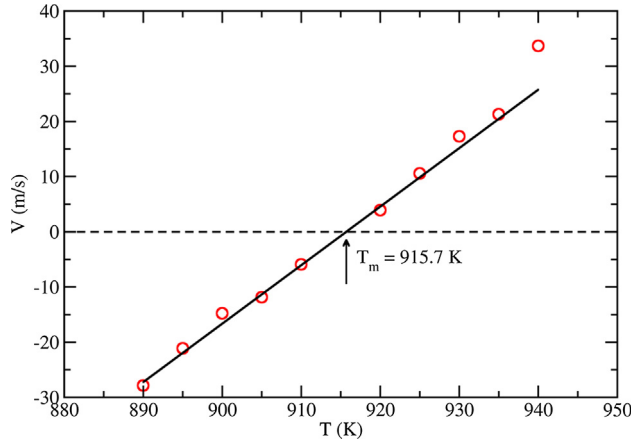

Fig. 3. The solid-liquid interface velocity for pure Al in the [1 0 0] direction as a function of temperature.

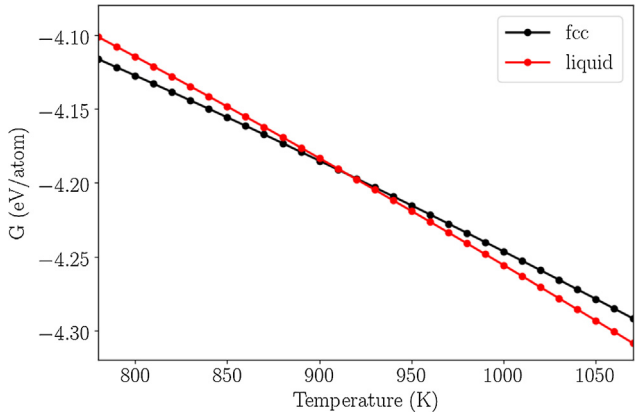

Fig. 4. Absolute Gibbs free energy of fcc and liquid Al as a function of temperature under the ambient pressure.

4. $Al_{1-x}Sm_x$ liquid

First, we introduce an auxiliary system $Al_{1-x}Sm'_x$, in which the factitious Sm′ atom has the mass of Sm but interacts with other atoms as Al. Thus, the Hamiltonian of $Al_{1-x}Sm'_x$ can be written as

$$H(p,q) = \sum_{i=1}^{3N(1-x)} \frac{p_i^2}{2m_{\mathrm{Al}}} + \sum_{i=1}^{3Nx} \frac{p_i^2}{2m_{\mathrm{Sm}}} + U_{\mathrm{Al}}(q), \tag{3}$$

where N is the number of atoms in the system, m_{Al} and m_{Sm} are the mass for Al and Sm atoms, respectively, and (p,q) refers to a point in the phase space $(p_1,p_2,\cdots,p_{3N},q_1,q_2,\cdots,q_{3N})$. The Helmholtz free energy for the liquid phase is defined as

$$\begin{aligned} F_{\mathrm{AlSm}} &= -k_{\mathrm{B}}T\ln\left\{\frac{1}{[N(1-x)]!\,(Nx)!\,h^{3N}}\int dpdqe^{-\beta H(p,q)}\right\} \\ &= -k_{\mathrm{B}}T\ln\left\{\frac{1}{[N(1-x)]!\,(Nx)!\,\Lambda_{\mathrm{Al}}^{3N(1-x)}\Lambda_{\mathrm{Sm}}^{3Nx}}\int dqe^{-\beta U_{\mathrm{Al}}(q)}\right\}, \end{aligned} \tag{4}$$

where $\beta = 1/k_{\mathrm{B}}T$, and Λ_α is the de Broglie wavelength for species α, which is defined as $\Lambda_\alpha = (h^2/2\pi m_\alpha k_{\mathrm{B}}T)^{1/2}$. For pure Al liquid,

$$F_{\mathrm{Al}} = -k_{\mathrm{B}}T\ln\left[\frac{1}{N!\Lambda_{\mathrm{Al}}^{3N}}\int dqe^{-\beta U_{\mathrm{Al}}(q)}\right]. \tag{5}$$

Comparing Eqs. (4) and (5), one can obtain the Helmholtz free energy difference between $Al_{1-x}Sm'_x$ liquid and pure Al liquid:

$$F_{\mathrm{AlSm}'} - F_{\mathrm{Al}} = Nk_{\mathrm{B}}T\left[\frac{3}{2}x\ln\frac{m_{\mathrm{Al}}}{m_{\mathrm{Sm}}} + x\ln x + (1-x)\ln(1-x)\right]. \tag{6}$$

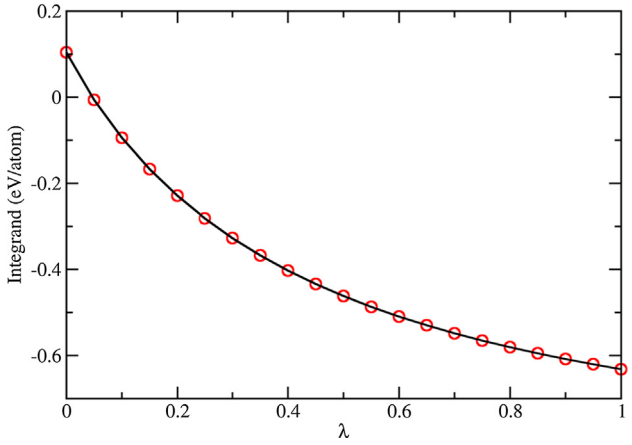

Fig. 5. The integrand of Eq. (7) for $x = 0.25$ and $T = 1500$ K. Open circles are data points collected in separated MD runs. The solid line is a cubic spline interpolation.

Since $Al_{1-x}Sm'_x$ liquid and pure Al liquid share the same interaction potential, the equilibrium volume should also be the same under the same pressure. Thus, Eq. (6) also describes the Gibbs free energy difference between the two systems (the PV term cancels out).

Next, we use TI to transform the factitious $Al_{1-x}Sm'_x$ system to the real $Al_{1-x}Sm_x$ system. To do that, we introduce intermediate systems interacting as $U(\lambda) = (1-\lambda)U_{\mathrm{Al}} + \lambda U_{\mathrm{AlSm}}$. Then, the difference in Gibbs free energy between the two systems can be expressed as

$$G_{\mathrm{AlSm}} - G_{\mathrm{AlSm}'} = \int_0^1 \left\langle \frac{dU(\lambda)}{d\lambda} \right\rangle_{\lambda,NPT} d\lambda = \int_0^1 \langle U_{\mathrm{AlSm}} - U_{\mathrm{Al}} \rangle_{\lambda,NPT}\, d\lambda, \tag{7}$$

where $\langle\cdots\rangle_{\lambda,NPT}$ stands for the isothermal-isobaric (NPT) ensemble average with respect to the intermediate potential $U(\lambda)$.

We use $x = 0.25$ and T= 1500 K as an example to describe the free energy calculation of liquid $Al_{1-x}Sm_x$ alloys. The transformation from Al liquid into the factitious Al-Sm′ liquid results in a free energy change $\Delta F = -0.156$ eV/atom, as calculated according to Eq. (6). The implementation of TI to transform Al-Sm′ into the real Al-Sm system is shown in Fig. 5, which gives $G_{\mathrm{AlSm}} - G_{\mathrm{AlSm}'} = -0.404$ eV/atom. Thus, the net difference of Gibbs free energy between the $Al_{0.75}Sm_{0.25}$ liquid and pure Al liquid is −0.560 eV/atom.

5. Applications

In the following, we demonstrate two applications of free energy calculations outlined in the above, namely, the determinations of driving force for fcc-Al nucleation in supercooled $Al_{1-x}Sm_x$ liquid and the melting curve for fcc-Al and Al_3Sm crystals.

5.1. *Driving force for nucleation of fcc-Al in supercooled* $Al_{1-x}Sm_x$ *liquid*

Crystal nucleation in supercooled liquid is an important process in numerous areas of physical science [36]. It is also an important factor for glass formation, since glass is formed by suppressing crystal nucleation during fast quenching. As a marginal glass former, the glass formability of Al-Sm has a strong dependence on the Sm concentration [37]. When as-quenched Al-Sm glass is gradually heated, the devitrification process often starts with the deposit of Al nanocrystals [38,39]. Thus, study of the effect of Sm concentration on Al nucleation in supercooled Al-Sm liquids can provide useful information for both glass formation and devitrification processes [40]. The driving force is a fundamental parameter that describes the net bulk free energy gain upon the formation of a crystalline nucleus. For fcc-Al nucleation in supercooled $Al_{1-x}Sm_x$ liquid, the driving force is defined as the free energy change in the liquid system when a single fcc-Al is nucleated

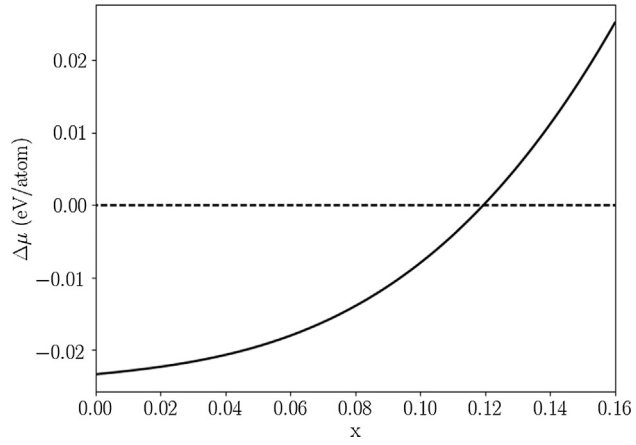

Fig. 6. Driving force for nucleation of fcc-Al in $Al_{1-x}Sm_x$ liquid at 700 K as a function of the Sm composition.

according to the "reaction" $N\,Al_{1-x}Sm_x \rightarrow Al_{fcc} + (N-1)Al_{1-x-\delta x}Sm_{x+\delta x}$, where N is the total number of atoms, and $\delta x = \frac{x}{N-1}$ based on mass conservation. Thus as $N \rightarrow \infty$,

$$\begin{aligned}\Delta\mu &= G_s + (N-1)G_l(x+\delta x) - NG_l(x)\\ &= G_s + (N-1)G_l(x) + (N-1)\tfrac{\partial G_l}{\partial x}\delta x - NG_l(x)\\ &= x\tfrac{\partial G_l}{\partial x} + G_s - G_l(x),\end{aligned} \tag{8}$$

where $G_l(x)$ and G_s refer to the Gibbs free energy per atom of $Al_{1-x}Sm_x$ liquid and fcc-Al, respectively. In Fig. 6, we plot $\Delta\mu$ as a function of x at a temperature of 700 K, where one can see that the driving force decreases as the Sm composition increases, but remains negative within the range of $x < 0.12$, showing that nucleation of fcc-Al is thermodynamically favored within this composition range. However, it should be noted that fcc-Al is the only solid phase considered in Fig. 6. When x becomes large (before reaching 0.12), nucleation of other solid phases such as Al_3Sm will become thermodynamically more favorable than fcc-Al.

5.2. *Melting curve (liquidus line) for fcc-Al and* Al_3Sm

We also perform the free-energy calculation for the hexagonal Al_3Sm phase, and traced out the melting curve (liquidus line) for both fcc-Al and Al_3Sm. We focus on the technologically important Al-rich region for this system, in which fcc-Al and Al_3Sm are the only two relevant solid phases according to the Al-Sm phase diagram [41,42]. Each coexistence point on the melting curve (x,T) of a solid phase denotes a coexistence state, which satisfies

$$(x-x_s)\frac{\partial G_l(x,T)}{\partial x} + G_s(T) = G_l(x,T) \tag{9}$$

where G_l and G_s are the Gibbs free energy of the liquid and solid phases, respectively, and x_s is the Sm composition in the solid phase. Mathematically, the coexistence composition at a specific temperature can be determined by the "tangent" construction as shown in Fig. 7, in which the formation Gibbs free energy of $Al_{1-x}Sm_x$ liquid G_f is plotted as a function of the Sm composition x, at a supercooled temperature of 880 K. G_f is calculated using the Gibbs free energy of fcc-Al and Al_3Sm at the same temperature as reference states. In this way, G_f for the two solid phases is zero (see Fig. 7). We construct tangential lines from the fcc-Al and Al_3Sm phases to the liquid curve, shown as the red and blue lines in Fig. 7, respectively. From the position of the tangential points, one can determine the coexistence liquid composition with the two solid phases to be 0.039 and 0.054, respectively.

The above procedure is repeated for various other temperatures to map out the melting curve for fcc-Al and Al_3Sm, as shown in Fig. 8. Our

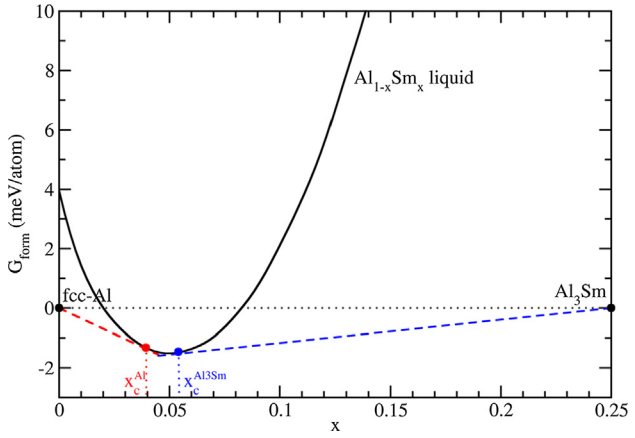

Fig. 7. The formation free energy of $Al_{1-x}Sm_x$ liquid, referenced to solid phases fcc-Al and Al_3Sm, at $T = 880$ K. The smooth curve is interpolated among 26 data points at increments of 0.01 using the cubic splining technique. The red and blue lines denote the tangential lines from fcc-Al and Al_3Sm to the liquid curve, respectively. The tangential points give the coexistence liquid composition with the two solid phases, respectively. (For interpretation of the references to colour in this figure legend, the reader is referred to the web version of this article.)

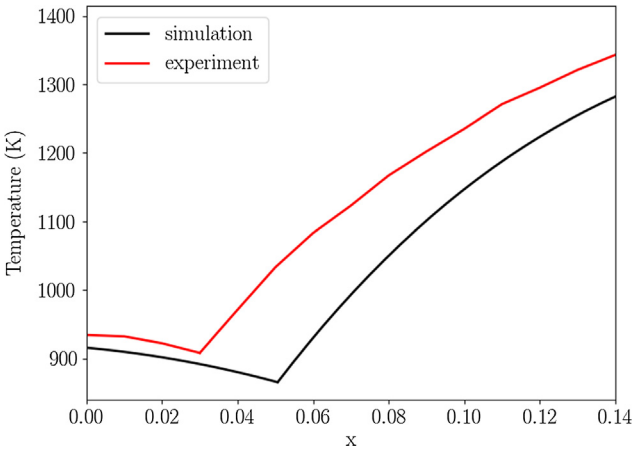

Fig. 8. Melting curve for fcc-Al and Al_3Sm from experiments [41,42] and the current calculations for $Al_{1-x}Sm_x$ in the Al-rich region of the Al-Sm system.

calculations predict a eutectic point at $T = 863$ K and $x = 0.051$, while the eutectic point from previous experiments [41,42] is located at $T = 908$ K and $x = 0.03$. At compositions away for the calculated eutectic point, our calculations generally underestimate the liquidus temperature by less than 100 K. Since the only energetics data used in fitting the Al-Sm FS potential was generated by density-functional theory (DFT) calculations at 0 K [33], we do expect some discrepancy with experiments in thermodynamic properties at finite temperatures. In this regard, a systematic way of determining solid-liquid phase equilibria, as outlined in the current paper, is valuable if one wants to refine a classical potential in order to more faithfully reproduce experimental thermodynamic information.

6. Conclusions

We establish a self-contained algorithm to rigorously evaluate the free energy for solid and liquid phases of an alloy system, based on thermodynamic integration. The algorithm starts from calculating the free energy of a single-element solid phase by referencing to a harmonic crystal. By monitoring the solid-liquid interface migration at different temperatures, we determine the melting point of the solid phase, which establishes a state of equality between the solid and liquid free energy.

The free energy difference at other state points between solid and liquid phases can be obtained by integrating $\Delta H/T^2$ with temperature, where ΔH is the latent heat during melting. Then, we generate an alchemical path connecting a pure liquid to a liquid alloy, and use thermodynamic integration to evaluate the mixing enthalpy and entropy. As an example, we apply this method on the Al-Sm system to determine the driving force for Al nucleation in Al-Sm liquid and the melting curve for the solid phases Al and Al_3Sm.

Data availability

The raw data (Al-Sm interatomic potential) required to reproduce these findings are available to download from https://www.ctcms.nist.gov/potentials/Al.html#Al-Sm.

Acknowledgements

This work was supported by the U.S. Department of Energy (DOE), Office of Science, Basic Energy Sciences, Materials Science and Engineering Division, including the grant of computer time at the National Energy Research Scientific Computing Center (NERSC) in Berkeley, CA. The research was performed at Ames Laboratory, which is operated for the U.S. DOE by Iowa State University under contract # DE-AC02-07CH11358. F.Z. and L.Y. also acknowledge the support by the Laboratory Directed Research and Development (LDRD) program of Ames Laboratory for developing software and performing computation with GPU acceleration.

References

[1] J.P. Hansen, D. Levesque, J. Zinn-Justin, Liquids, Freezing, and the Glass Transition, Les Houches session 51, North-Holland, Amsterdam, Amsterdam, 1991.
[2] D. Frenkel, B. Smit, Understanding Molecular Simulation: From Algorithms to Application, Academic Press, 2007.
[3] R.W. Zwanzig, High-temperature equation of state by a perturbation method. I. Nonpolar gases, J. Chem. Phys. 22 (1954) 1420–1426, http://dx.doi.org/10.1063/1.1740409.
[4] B. Widom, Some topics in the theory of fluids, J. Chem. Phys. 39 (1963) 2808–2812, http://dx.doi.org/10.1063/1.1734110.
[5] I. Nezbeda, J. Kolafa, A new version of the insertion particle method for determining the chemical potential by monte carlo simulation, Mol. Simul. 5 (1991) 391–403, http://dx.doi.org/10.1080/08927029108022424.
[6] M. Athènes, Computation of a chemical potential using a residence weight algorithm, Phys. Rev. E - Stat. Physics, Plasmas, Fluids, Relat. Interdiscip. Top. 66 (2002) 14, http://dx.doi.org/10.1103/PhysRevE.66.046705.
[7] J.G. Kirkwood, Statistical mechanics of fluid mixtures, J. Chem. Phys. 3 (1935) 300–313, http://dx.doi.org/10.1063/1.1749657.
[8] C.H. Bennett, Efficient estimation of free energy differences from Monte Carlo data, J. Comput. Phys. 22 (1976) 245–268, http://dx.doi.org/10.1016/0021-9991(76)90078-4.
[9] N. Lu, J.K. Singh, D.A. Kofke, Appropriate methods to combine forward and reverse free-energy perturbation averages, J. Chem. Phys. 118 (2003) 2977–2984, http://dx.doi.org/10.1063/1.1537241.
[10] S. Kumar, J.M. Rosenberg, D. Bouzida, R.H. Swendsen, P.A. Kollman, THE weighted histogram analysis method for free-energy calculations on biomolecules. I. The method, J. Comput. Chem. 13 (1992) 1011–1021, http://dx.doi.org/10.1002/jcc.540130812.
[11] G.M.G.M.M.J.P.J.P.P. Torrie, Valleau Nonphysical sampling distributions in Monte Carlo free-energy estimation: Umbrella sampling, J. Comput. Phys. 23 (1977) 187–199, http://dx.doi.org/10.1016/0021-9991(77)90121-8.
[12] M. Watanabe, W.P. Reinhardt, Direct dynamical calculation of entropy and free energy by adiabatic switching, Phys. Rev. Lett. 65 (1990) 3301–3304, http://dx.doi.org/10.1103/PhysRevLett. 65.3301.
[13] G. Adjanor, M. Athènes, Gibbs free-energy estimates from direct path-sampling computations, J. Chem. Phys. 123 (2005), http://dx.doi.org/10.1063/1.2137698.
[14] G. Adjanor, M. Athenes, F. Calvo, Free energy landscape from path-sampling: application to the structural transition in LJ(38), Eur. Phys. J. B 53 (2006) 47–60, http://dx.doi.org/10.1140/epjb/e2006-00353-0.
[15] G. Adjanor, M. Athènes, Thermodynamic modelling of glasses at atomistic scale, AIP Conf. Proc. 999 (2008) 186–201, http://dx.doi.org/10.1063/1.2918104.
[16] G. Adjanor, M. Athènes, J.M. Rodgers, Waste-recycling Monte Carlo with optimal estimates: Application to free energy calculations in alloys, J. Chem. Phys. 135 (2011), http://dx.doi.org/10.1063/1.3610423.
[17] H. Do, J.D. Hirst, R.J. Wheatley, Calculation of partition functions and free energies of a binary mixture using the energy partitioning method: application to carbon dioxide and methane, J. Phys. Chem. B 116 (2012) 4535–4542, http://dx.doi.org/10.1021/jp212168f.
[18] K.G.S.H. Gunawardana, S.R. Wilson, M.I. Mendelev, X. Song, Theoretical calculation of the melting curve of Cu-Zr binary alloys, Phys. Rev. E - Stat. Nonlinear, Soft Matter Phys. 90 (2014) 1–8, http://dx.doi.org/10.1103/PhysRevE.90.052403.
[19] S. Plimpton, Fast parallel algorithms for short-range molecular dynamics, J. Comput. Phys. 117 (1995) 1–19, http://dx.doi.org/10.1006/jcph.1995.1039.
[20] W.M. Brown, P. Wang, S.J. Plimpton, A.N. Tharrington, Implementing molecular dynamics on hybrid high performance computers - Short range forces, Comput. Phys. Commun. 182 (2011) 898–911, http://dx.doi.org/10.1016/j.cpc.2010.12.021.
[21] D. Frenkel, A.J.C. Ladd, New Monte Carlo method to compute the free energy of arbitrary solids. Application to the fcc and hcp phases of hard spheres, J. Chem. Phys. 81 (1984) 3188–3193, http://dx.doi.org/10.1063/1.448024.
[22] M. de Koning, A. Antonelli, Einstein crystal as a reference system in free energy estimation using adiabatic switching, Phys. Rev. E 53 (1996) 465–474, http://dx.doi.org/10.1103/PhysRevE.53.465.
[23] D.M. Eike, E.J. Maginn, Atomistic simulation of solid-liquid coexistence for molecular systems: application to triazole and benzene, J. Chem. Phys. 124 (2006), http://dx.doi.org/10.1063/1.2188400.
[24] G. Grochola, Constrained fluid λ-integration: constructing a reversible thermodynamic path between the solid and liquid state, J. Chem. Phys. 120 (2004) 2122–2126, http://dx.doi.org/10.1063/1.1637575.
[25] D.M. Eike, J.F. Brennecke, E.J. Maginn, Toward a robust and general molecular simulation method for computing solid-liquid coexistence, J. Chem. Phys. 122 (2005), http://dx.doi.org/10.1063/1.1823371.
[26] T.P. Straatsma, J.A. McCammon, Multiconfiguration thermodynamic integration, J. Chem. Phys. 95 (1991) 1175–1188, http://dx.doi.org/10.1063/1.461148.
[27] A. Blondel, Ensemble variance in free energy calculations by thermodynamic integration: theory, optimal “Alchemical” path, and practical solutions, J. Comput. Chem. 25 (2004) 985–993, http://dx.doi.org/10.1002/jcc.20025.
[28] T.S. Lee, Y. Hu, B. Sherborne, Z. Guo, D.M. York, Toward fast and accurate binding affinity prediction with pmemdGTI: an efficient implementation of GPU-accelerated thermodynamic integration, J. Chem. Theory Comput. 13 (2017) 3077–3084, http://dx.doi.org/10.1021/acs.jctc.7b00102.
[29] N. Wang, Y.E. Kalay, R. Trivedi, Eutectic-to-metallic glass transition in the Al–Sm system, Acta Mater. 59 (2011) 6604–6619, http://dx.doi.org/10.1016/j.actamat.2011.07.015.
[30] W.G. Hoover, Canonical dynamics: equilibrium phase-space distributions, Phys. Rev. A 31 (1985) 1695.
[31] G.J. Martyna, M.L. Klein, M. Tuckerman, Nosé-Hoover chains: the canonical ensemble via continuous dynamics, J. Chem. Phys. 97 (1992) 2635–2643, http://dx.doi.org/10.1063/1.463940.
[32] M.W. Finnis, J.E. Sinclair, A simple empirical N-body potential for transition metals, Philos. Mag. A 50 (1984) 45–55.
[33] M.I. Mendelev, F. Zhang, Z. Ye, Y. Sun, M.C. Nguyen, S.R. Wilson, C.Z. Wang, K.M. Ho, Development of interatomic potentials appropriate for simulation of devitrification of $Al_{90}Sm_{10}$ alloy, Model. Simul. Mater. Sci. Eng. 23 (2015), http://dx.doi.org/10.1088/0965-0393/23/4/045013.
[34] M. Kresch, M. Lucas, O. Delaire, J.Y.Y. Lin, B. Fultz, Phonons in aluminum at high temperatures studied by inelastic neutron scattering, Phys. Rev. B – Condens. Matter Mater. Phys. 77 (2008) 1–9, http://dx.doi.org/10.1103/PhysRevB.77.024301.
[35] S.R. Wilson, K.G.S.H. Gunawardana, M.I. Mendelev, Solid-liquid interface free energies of pure bcc metals and B2 phases Solid-liquid interface free energies of pure bcc metals and B2 phases, 134705 (2016). doi: 10.1063/1.4916741.
[36] K.F. Kelton, A.L.A.L. Greer, Nucleation in Condensed Matter: Application in Materials and Biology, Elsevier, Amsterdam, 2010.
[37] A. Inoue, Amorphous, nanoquasicrystalline and nanocrystalline alloys in Al-based systems, Prog. Mater Sci. 43 (1998) 365–520.
[38] P. Rizzi, M. Baricco, S. Borace, L. Battezzati, Phase selection in Al-TM-RE alloys: nanocrystalline Al versus intermetallics, Mater. Sci. Eng., A 304–306 (2001) 574–578, http://dx.doi.org/10.1016/S0921-5093(00)01537-9.
[39] Z. Ye, F. Zhang, Y. Sun, M.I. Mendelev, R.T. Ott, E. Park, M.F. Besser, M.J. Kramer, Z. Ding, C.-Z. Wang, K.-M. Ho, Discovery of a metastable Al20Sm4 phase, Appl. Phys. Lett. 106 (2015) 101903, http://dx.doi.org/10.1063/1.4914399.
[40] G.B. Bokas, L. Zhao, J.H. Perepezko, I. Szlufarska, On the role of Sm in solidification of Al-Sm metallic glasses, Scr. Mater. 124 (2016) 99–102, http://dx.doi.org/10.1016/j.scriptamat.2016.06.045.
[41] V.I. Kononenko, S.V. Golubev, On phase diagrams for binary systems of aluminium with la ce p, Izv. Akad. Nauk SSSR, Met., 1990, pp. 197–199.
[42] A. Saccone, G. Cacciamani, D. Maccio, G. Borzone, R. Ferro, D. Macciò, G. Borzone, R. Ferro, Contribution to the study of the alloys and intermetallic compounds of aluminium with the rare-earth metals, Intermetallics 6 (1998) 201–215, http://dx.doi.org/10.1016/S0966-9795(97)00066-6.